REVISION 1

Relaxation effects and re-entrant spin glass behaviour at low temperatures in natural strunzite, ferristrunzite and ferrostrunzite

Antoine Van Alboom[1,2,*] and Eddy De Grave[2]

[1] Physics, Faculty of Applied Engineering Sciences, University College Gent, Valentin Vaerwyckweg 1, 9000 Gent, Belgium

[2] NUMAT, Department of Subatomic and Radiation Physics, University of Gent, Proeftuinstraat 86, 9000 Gent, Belgium

* Present adress : Physics, Faculty of Applied Engineering Sciences, University College Gent, Valentin Vaerwyckweg 1, 9000 Gent, Belgium. E-mail: toon.vanalboom@hogent.be

Keywords: strunzite, ferristunzite, ferrostrunzite, Mössbauer spectroscopy, hyperfine field

Abstract

The temperature variations of the ferric and ferrous hyperfine fields in natural samples of strunzite, ferristrunzite and ferrostrunzite are examined by Mössbauer spectroscopy between 4.2 K and their respective magnetic transition temperatures. The spectra of all three strunzite species are composed of two dominant sextets with equal contribution and with hyperfine fields at 4.2 K of approximately 48.5 T and 48.0 T, respectively. They are assigned to Fe^{3+} cations in the Fe(1) and Fe(2) sites in the crystallographic structure. A third magnetic component, with field of 54.8 T ± 0.1 T, is well resolved in the 4.2 K spectrum of ferristrunzite and is attributed to Fe^{3+} in the Mn sites of the structure. This third ferric contribution also appears in the spectra of strunzite and ferrostrunzite, however with smaller relative spectral areas as compared to ferristrunzite, i.e., ~10% and ~3% of total spectral area, respectively, where it is 30% for ferristrunzite. For ferrostrunzite, two additional magnetic components are recognized. They are both attributed to Fe^{2+} substituting in the Mn sites.

Their hyperfine fields at 4.2 K are 21.8 T ± 0.5 T and 28.6 T ± 0.5 T, respectively, and their relative contributions 11% and 15%. With increasing temperature, enhanced asymmetric broadening of the absorption lines is observed for all three samples. This phenomenon is due to relaxation of the magnetic moments, thus causing gradually broader distribution ranges of the respective hyperfine fields. The spectra have been fitted with superpositions of model-independent hyperfine-field distributions. The temperature dependencies of the maximum-probability hyperfine fields of the two ferric subspectra associated with the Fe(1) and Fe(2) sites are interpreted in terms of the molecular field theory taking into account the occurrence of exchange magnetostriction. The variations with temperature of the magnetic hyperfine fields acting at the Mn sites indicate that the magnetization of the Mn sublattice shows re-entrant spin glass behaviour. This feature is most prominent for the strunzite sample.

1. Introduction

Strunzite, ferristrunzite and ferrostrunzite are three isostructural minerals with triclinic crystallographic structure (P1) (Frondel 1957, Fanfani et al. 1978, Peacor et al. 1983). The ideal chemical formulas are $Mn^{2+}Fe^{3+}{}_2(PO_4)_2(OH)_2{\cdot}6(H_2O)$, $Fe^{3+}Fe^{3+}{}_2(PO_4)_2(OH)_2{\cdot}[(H_2O)_5(OH)]$ (Vochten and De Grave 1990) and $Fe^{2+}Fe^{3+}{}_2(PO_4)_2(OH)_2{\cdot}6(H_2O)$ (Vochten et al. 1995), respectively. Ferristrunzite may be regarded as the fully oxidized form of ferrostrunzite.

The strunzite structure (Figure 1) consists of infinite chains of octahedral ferric sites along the c axis which are linked to one another by sharing hydroxyl groups and by PO_4 tetrahedra. The latter also bind adjacent chains, thus forming slabs that are connected to each other by Mn octahedra between remaining PO_4 vertices. Within the chains two ferric sites Fe(1) and Fe(2) alternate, of which Fe(1) is somewhat more distorted than Fe(2) as indicated by a slight difference in average Fe-O bond length and average O-Fe-O bond angle (Vochten and De Grave 1990). The crystallographic unit cell contains two octahedra of each type.

In ferristrunzite the manganese is substituted by Fe^{3+}, in ferrostrunzite by Fe^{2+}. In the first case the charge balance is re-established by substitution of an H_2O by an OH^- at a non-bridging vertex of the Mn octahedron. In the following, this position is referred to as the Mn site.

Mössbauer spectra (MS) at room temperature (RT) and at 4.2 K for these three mineral species have been reported earlier (Vochten and De Grave 1990, Vochten et al. 1995, Van Tassel and De Grave 1992). In this paper the detailed temperature dependencies of the Mössbauer parameters between 4.2 K and their respective magnetic transition temperatures (T_N) are presented and discussed, with emphasis on the magnetic hyperfine fields, in order to gain an insight into the relation between the crystallographic structure and the magnetic properties of these minerals.

Preliminary numerical results were reported earlier (Van Alboom and De Grave 2005). However, the data at that time could not be explained satisfactorily and no sound conclusions were drawn.

2. Experimental

The samples used in this study were described earlier (Vochten and De Grave 1990, Vochten et al. 1995, Van Tassel and De Grave 1992) and were characterised by these authors using X-ray diffraction, chemical analysis and Mössbauer spectroscopy at room temperature (RT) and 4.2 K.

In the present work, Mössbauer spectra for powder samples were collected at variable temperatures in the range where the samples exhibit magnetic ordering. Prior to these experiments, the respective magnetic order-disorder transition temperatures (T_N) were determined by the Mössbauer thermoscanning technique, in which the temperature (T) variation of the γ-ray transmission through the absorber is recorded with the source at zero velocity (Chambaere and De Grave 1984).

For the acquisition of MS conventional time-mode spectrometers were used operating with a triangular reference signal. The sources were ^{57}Co in Rh matrix, but all center shift (δ) values quoted hereafter are relative to α-Fe at room temperature.

The obtained spectra were numerically analyzed assuming either discrete Lorentzian-shaped magnetic components (fitting program referred to hereafter as SFP) or, where found to be recommended, by model-independent distributions (Vandenberghe et al. 1994) of such components (program DFP). The positions and intensities of the various absorption lines were calculated by diagonalization of the full nuclear interaction hamiltonian (Hoy and Chandra 1967, Kündig 1967). Most generally, a magnetically split ^{57}Fe-MS contains a maximum of eight absorption lines of which the respective positions are determined by the so-called Mössbauer parameters, particularly: the center shift δ, the hyperfine field B_{hf} and the polar (Ω) and the azimuthal angle (Ψ) of the hyperfine field in the principal axis system (x,y,z) of the electric field gradient (EFG) with components (V_{xx}, V_{yy}, V_{zz}). Finally, two additional parameters, related to the quadrupole interaction, affect the line positions, i.e., the quadrupole splitting ΔE_Q and the asymmetry parameter η. They are given by, respectively,

$$\Delta E_Q = \frac{1}{2} e^2 qQ = \frac{1}{2} V_{zz} eQ, \tag{1}$$

and

$$\eta = \frac{V_{xx} - V_{yy}}{V_{zz}}, \tag{2}$$

with V_{zz} the principal EFG component and Q the nuclear quadrupole moment.

However, in the case of Fe^{3+} the quadrupole interaction is generally weak in comparison with the magnetic dipole interaction. As a result, the peak positions are not independently determined by ΔE_Q and Ω, but instead by the quadrupole shift ($2\varepsilon_Q$), which is given by

$$2\varepsilon_Q = \frac{1}{2}\Delta E_Q(3\cos^2\Omega - 1)\,. \quad (3)$$

Further in this case, the number of lines is reduced to six (sextet) with ideally a mutual line-intensity ratio of 3:2:1:1:2:3 for a random-powder absorber.

In addition to the above mentioned parameters the line width (Γ: full width at half maximum height) and the relative area (*RA*) for each spectral component appearing in a multi-phase spectrum are determined by fitting the experimental MS.

Because of the diversity in types of Mössbauer spectra, four different fitting programs were used in this study. SFP1 and SFP2 (single component fit programs) were aimed to analyse MS consisting of a superposition of a number of well-defined discrete magnetically split subspectra, which are composed of only one subcomponent. Distribution fit programs (DFP1 and DFP2) were applied if subspectra themselves were the superposition of a number of magnetically split subcomponents related to a distribution of hyperfine fields. In these cases, only model independent distributions of hyperfine fields (Vandenberghe et al. 1994) were considered. In SFP1 and DFP1, the positions of the absorption lines (either discrete sextets or distributions of sextets, respectively) are calculated from their analytical expressions as function of the various Mössbauer parameters. This approach applies to Fe sites for which the quadrupole interaction is weak compared to the magnetic hyperfine interaction. If the latter condition is not met, the programs SFP2 and DFP2 are used which are both based on the diagonalization of the full nuclear interaction hamiltonian.

3. Mössbauer analysis

3.1 Thermoscanning

The Mössbauer thermoscanning curves for the three strunzite varieties are reproduced in Figure 2. Expanding on previously reported data (Van Alboom and De Grave 2005), the magnetic order-disorder transition temperatures were accurately and consistently determined, yielding the values 50.5 ± 0.5 K, 44 ± 1 K and 45 ± 3 K for respectively strunzite,

ferristrunzite and ferrostrunzite. Hence, the Fe-for-Mn substitution in the strunzite structure seems to weaken the strength of the overall magnetic exchange interaction. The T_N-value as determined from thermoscanning gives an overall value for a sample, and therefore does not correspond necessarily to the values of all the magnetic sublattices of the sample.

3.2 Ferristrunzite

At 4.2 K the experimental MS of ferristrunzite was satisfactorily described using SFP1 assuming a superposition of three ferric Lorentzian shaped sextets, S1, S2, and S3 (Vochten and De Grave 1990), attributed to the three distinct Fe sites available in the ferristrunzite structure. The respective center shift values are very similar ($\delta \approx 0.50$ mm/s) and are consistent with an octahedral co-ordination.

Two of these sextets (S1 and S2) have slightly different hyperfine fields (B_{hf} = 48.4 T ± 0.1 T and B_{hf} = 47.8 T ± 0.1 T) while the third one (S3) has a remarkably higher hyperfine field (B_{hf} = 54.8 T ± 0.1 T) at 4.2 K. S1 and S2 are assigned to Fe^{3+} at the Fe(1 or 2) and Fe(2 or 1) sites in the structure. Although the quadrupole shifts for Fe^{3+}(S1) and Fe^{3+}(S2) are different, further unambiguous assignment to the Fe(1) or Fe(2) sites isn't possible, because the difference in $2\varepsilon_Q$ is related to the difference in orientation of the local hyperfine field with respect to the local EFG in both sites, of which the orientation isn't known until now. S3 is attributed to Fe^{3+} at the Mn position. The center shifts corresponding to S1 and S2 were constrained to have equal values. The subspectral area fractions were fixed on the ratio 0.35:0.35:0.30 which corresponds to a model for which the aluminum, which was detected by EDX to be present in the sample by an amount of 0.10 per formula unit, is located on the Mn sites in the structure. It was experienced, however, that a forced random distribution of the Al among the three available lattice sites or among sites Fe(1) and Fe(2) did not significantly affect the adjusted hyperfine parameter values. The line area ratios 3:*x*:*y* of the outer to middle to inner lines for a particular subspectrum were assumed to be the same for all three

components and were found to be 3:2.43:1.14. The deviation from the ideal 3:2:1 ratio can be due to thickness effects or texture effects, however here, also relaxation effects cannot be excluded (see further). As it is experienced that the deviation is irrelevant for the subsequent determination and interpretation of the temperature variations of the various hyperfine parameters, the hyperfine field in particular, no further attention is paid to the line area ratios.

At 8 K and higher temperatures *T*, significant line broadening is noticed, as well as additional absorption at low velocities which becomes more prominent with increasing *T*. It was found that its contribution could be taken into account by introducing an extra doublet component D1 in the foregoing analyzing procedure, hereby keeping the same constraints for the sextets as those imposed on the fit of the 4.2 K spectrum. The adjusted values of the D1 center shift values are, within experimental error limits, equal to those of the sextet components. Further, the MS acquired at 8 K and 14 K show strongly overlapping sextet subspectra S1, S2, and S3 and consequently their Mössbauer parameters could not be determined accurately using the SFP1 fitting approach. Nevertheless, a remarkably different *T*-dependence of the hyperfine fields among these subspectra is observed. While $B_{\mathrm{hf,S1}}$ and $B_{\mathrm{hf,S2}}$ show nearly the same *T*-dependence, $B_{\mathrm{hf,S3}}$ decreases more rapidly with increasing *T* than $B_{\mathrm{hf,S1}}$ and $B_{\mathrm{hf,S2}}$ and above 14 K the field $B_{\mathrm{hf,S3}}$ becomes smaller than the corresponding S1 and S2 values.

From 17 K on, the asymmetric broadening of the absorption lines is considerable and increases drastically with increasing *T*. As a result, the analysis of these MS using a superposition of three discrete sextets and one doublet (SFP1 approach) failed. Therefore, the theoretical spectra were calculated by the superposition of three model independent distributions of hyperfine fields, respectively, related to the already mentioned Fe sites, using the distribution fitting program DFP1. In this case, a subspectrum is generally the superposition of a certain number of subcomponents (given by #div), of which the hyperfine

fields have different values as given by the distribution, whereas the center shifts, the quadrupole shifts, the line widths and the corresponding line area ratios are constraint to equal values for all subcomponents. Here the line area ratios of all these subcomponents were fixed at 3:2:1. The central component D1 was fitted as a discrete, Lorentzian-shaped quadrupole doublet. At 17 K and higher *T*, the center shifts of all subspectra were constrained to have equal values. Regrettably, in the minimization routine used in the distribution program for fitting the MS, it is not possible to impose fixed values for the *RA* of the subspectra. Such possibility would indeed be very useful when strongly overlapping subspectra determine the overall Mössbauer line shape. As a consequence and also because of the nearly total overlap of S1 and S2, the RA results for S1 and S2 fluctuated strongly depending on the input parameter values. Therefore, at each *T*, several trial fits were done with different distribution ranges (lower and upper limits for the allowed hyperfine fields) and/or different fixed $2\varepsilon_Q$ values for S1 and S2 in order to get nearly equal RA values for S1 and S2. It was found that fixing or not fixing the elemental line width Γ, only slightly affected the adjusted RA values, while the positions of the respective maximum probability hyperfine fields did not change substantially.

Applying the calculation approaches as outlined above, the MS at temperatures between 4.2 K and T_N could satisfactorily be reproduced. Figure 3 shows selected experimental and calculated spectra as well as the probability distribution profiles $p(B_{hf})$ of the three sextet components. It is noticed that the $p(B_{hf})$ profiles for S1 and S2 are very close to one another, both in shape and in probability for a given field value. In spite of the strong overlap of the sextet components at higher *T*, and hence their ill-defined parameter values, reasonably consistent results for these parameters were obtained, especially for the hyperfine fields B_{max} at maximum probability.

Table I gives the results of the relevant Mössbauer parameters for which the *RA* of the S1 and S2 components are in good approximation the same and for which the Mössbauer parameters of all the subspectra show a consistent and physical acceptable dependence of temperature. The quadrupole shifts of the various sextets are not sharply defined, but it is clear that their values for S1 and S2 have opposite signs. Figure 3 contains the experimental and calculated MS. At 17 K and higher *T*, the *RA* of S1 and S2 decrease substantially.

The quadrupole splitting of component D1 was determined for all *T* to be approximately 0.75mm/s, which is in good agreement with the value of the quadrupole splitting of the doublet absorption at maximum probability above T_N (Vochten and De Grave 1990). $2\varepsilon_{Q,S1}$ and $2\varepsilon_{Q,S2}$ had always a different sign, and vary between –0.63 and –0.42 mm/s for S1 and between 0.11 and 0.32 mm/s for S2. Most probably these fluctuations are a consequence of the overlap of S1 and S2, by which it was not possible to determine these values more precisely. A change in sign of $2\varepsilon_{Q,S3}$ below 8 K and above 14 K is determined. Because the sign of $2\varepsilon_Q$ is related to the orientation of the local hyperfine field to the principal axis of the EFG, the difference in sign of $2\varepsilon_{Q,S1}$ and $2\varepsilon_{Q,S2}$ indicates a difference in that orientation at Fe(1) and Fe(2) sites. For the same reason the difference in sign of $2\varepsilon_{Q,S3}$ below 8 K and above 14 K should be interpreted as a change in the direction of the local hyperfine field with respect to the principal axis of the local EFG. However, taking into account the constraints on some of the parameters during the analysis, one best takes any reservation concerning this finding.

The effect of increasing RA_{D1} and decreasing *RA* of the other components with increasing *T* above 17 K, is interpreted in the context of relaxation of the magnetic moments, by which the magnetic moments remain increasingly less time in their equilibrium positions as *T* increases. When the relaxation time is sufficiently shorter than the nuclear Larmor precession time (of the order 10^{-7} s), then the Mössbauer absorption is of doublet type. In the opposite case, when

the magnetic moments stay long enough in their equilibrium state, one observes a magnetically split spectrum. In the intermediate case, the absorption manifests itself as the superposition of a continuum of hyperfine fields between 0 T (doublet situation) and a maximum value.

From these considerations, the D1 component has to be associated with Fe^{3+} for which the relaxation time is already short enough to get a more doublet-like absorption. That the relaxation phenomenon is spread over a relatively wide temperature range, means that the magnetic exchange interaction with neighbouring magnetic ions, which is responsible for the orientation of the magnetic moments, is not equally strong at each site, and being weakest for Fe^{3+} at Mn sites. This last assertion can be easily understood because the Mn site in strunzite is a relatively isolated octahedrally co-ordinated site between the slabs of chains of octahedral ferric sites in the crystallographic structure. Therefore it is plausible that the Fe^{3+} at the Mn position has weaker magnetic exchange interactions with neighbouring magnetic ions than $Fe^{3+}(1)$ and $Fe^{3+}(2)$ do.

The broadening of the absorption lines is interpreted as being the consequence of local differences in the strength of the magnetic exchange interactions between neighbouring magnetic ions caused by local differences in the co-ordination of the probe ions. Consequently the T-dependence of the hyperfine field at a certain position can be different from the one at another position of the same site, whereas the saturation values at lowest T are approximately the same. In the former case, a broad B_{hf} distribution range arises and an asymmetric broadening of the outer absorption lines of the spectral component is observed when T increases. In order to analyse spectra showing relaxation effects, a special fitting routine is designed in the past (Blume and Tjon 1968), which is successfully applied to Mössbauer spectra with single component subspectra. However because of the strong overlap of the

subspectra, which themselves show a distribution of hyperfine fields, this fitting routine is not applicable for the minerals in this study.

3.3 Strunzite

Using SFP1 the MS of strunzite at 4.2 K was calculated by three sextets and an additional doublet component D2 at small velocities with *RA* less than 3 %. This doublet was assigned to some iron in the window of the equipment. The center shifts and line widths of S1 and S2 were constrained to equal values. Broadening of the outer lines of these components was taken into account by a linear broadening parameter ($\Delta\Gamma$): the inner line to middle to outer lines having line widths Γ , $\Gamma+\Delta\Gamma$ and $\Gamma+2\Delta\Gamma$. Additionally a coupled 3:*x*:1 ratio for the line area of the sextet absorption lines was used. In this way the MS was satisfactorilly reproduced and the results for the Mössbauer parameters of the sextets at 4.2 K (see Table II) were very similar to those at 4.2 K in ferristrunzite. In comparison with ferristrunzite and the components S1 and S2, the component with the highest B_{hf} (S3) had now a substantially smaller area fraction of 0.11 approximately, S1 and S2 having equal area fractions of 0.44 approximately. However the sign of $2\varepsilon_{Q,S3}$ at 4.2 K in strunzite was opposite to the corresponding one in ferristrunzite.

The MS at 10 K was also satisfactorilly reproduced by an analogous superposition of discrete components for which the *RA* of the sextets were fixed at 0.44:0.44:0.11 and the Mössbauer parameters of D2 at the 4.2 K values (except the line width). In this case S3 overlapped totally with S1 and S2, and its parameters therefore are somewhat more inaccurate.

At increasing temperatures, $B_{hf,S3}$ decreased very rapidly and already at 15 K, its value was much smaller than $B_{hf,S1}$ and $B_{hf,S2}$. Meanwhile, using SFP1, the line width of S3 increased strongly with increasing *T*, most probably because of relaxation effects. Therefore, from 15 K and higher *T*, the MS were analysed using DFP1 with the distribution fitting model for S3, whereas S1 and S2 were reproduced by discrete sextet components with a coupled linear

broadening of the absorption lines. All sextet components were constrained to equal 3:*x*:1 line area ratios and to equal center shifts. However DFP1 has the disadvantage that the relative areas of the components could not be fixed. Up to 20 K the parameters of D2 were fixed to the values found at 4.2 K. Above 20 K up to 47 K the lower limit of the distribution range for $B_{hf,S3}$ was lowered to 0 and consequently overlapped the absorption corresponding to D2. A separate D2 doublet therefore was not taken into consideration for these *T*. At 43 and 47 K the MS showed also asymmetric broadening for the S1 and S2 absorption. Therefore these MS were reproduced using DFP1 with distribution models for the hyperfine fields related to the S1, S2 and S3 absorption. At 47 K additional doublet absorption D1 was resolved. As for ferristrunzite, at each *T*, several fits were done with different distribution ranges and/or different fixed $2\varepsilon_Q$ values for S1 and S2 in order to get nearly equal RA for S1 and S2. Again it was clear that the dominating sextet absorption was the superposition of two components with very similar hyperfine field distributions and with a different sign for the related quadrupole shifts, indicating that the hyperfine field orientation is different with respect to the local principal axis of the EFG at the corresponding sites. At 43 K and at 47 K the subspectra in the MS are clearly collapsing and at these *T*, the highest value of the hyperfine field distribution of S3 was only 12.0 T and 10.0 T, respectively. The results for which the *RA* of the S1 and S2 components are in good approximation the same and for which the Mössbauer parameters of all the subspectra show a consistent and physical acceptable dependence of temperature, are given in Table II. Figure 4 contains the experimental and calculated MS.

3.4 Ferrostrunzite

In the MS of ferrostrunzite below T_N = 45 ± 3 K, because of the presence of Fe^{2+} in the sample, magnetically split ferrous subspectra were observed in addition to the Fe^{3+} subspectra. Because for Fe^{2+}, the quadrupole interaction and the magnetic dipole interaction are of the same order, the MS of ferrostrunzite below T_N were analysed with the method based

on the diagonalization of the full nuclear interaction hamiltonian. At 5 K the MS could be reproduced by three discrete ferric (sextet) and two ferrous magnetically split subspectra using SFP2. A position dependent width broadening parameter ($\Delta\Gamma$) accounts for some broadening of the outher lines caused by small local variations of B_{hf}. As for the other samples, two of these ferric subspectra (S1 and S2) are related to Fe^{3+} at the Fe(1 or 2) and Fe(2 or 1) sites and the third ferric component (S3) is assigned to ferric ions at the Mn site. Keeping the area fractions of S1 and S2 equal to each other during the fitting process gives no worse goodness-of-fit values, thus makes an equal ferric occupation of both sites very plausible. Because the ferrous quadrupole splitting is temperature dependent as consequence of the varying Boltzmann occupation of the lower ^{5}D orbital electron energy levels, its value saturates at low temperatures; this occurs already at about 80 K. From this consideration, quadrupole splittings of the two ferrous magnetically split subspectra (S4 and S5) were fixed at the values just above the magnetic transition temperature, 3.04 and 2.52 mm/s respectively (Van Tassel and De Grave 1992). The area fractions of both ferrous subspectra were fixed at the ratio determined just above the magnetic transition temperature. This was also done for the center shifts of both components.

At 22 K and 28 K an asymmetric broadening of the outer absorption peaks was visually observed, indicating an inhomogeneous hyperfine field decrease at Fe(1) and Fe(2) sites. Therefore, at these temperatures, the MS were analysed using ferric subspectra with distributions of hyperfine fields. Also an increase of the absorption near zero velocity was observed and S3 could not be resolved anymore. In order to reproduce the MS at these T, therefore a magnetically split subspectrum (S6) was added, for which the hyperfine field range extends from 0.0 to 10.0 T. The quadrupole shift of it was fixed at the value of 0.755 mm/s for the quadrupole splitting with highest probability in the paramagnetic spectrum just above T_N (Van Tassel and De Grave 1992). Because of the strong overlap of the subspectra,

by which their resolution is strongly limited, the S6 absorption is composed of the collapsing S3 on the one hand, and parts of the S1 and S2 absorption on the other hand. Center shifts and widths of the ferric subspectra were constrained to equal values. Because of the strong overlap with the other subspectra, the ferrous absorption was reproduced by single magnetically split subspectra with large line widths constrained equal to each other. For the calculations at these *T*, DFP2 was used. However relative areas could not be fixed, and because of the strong overlap with the ferric subspectra, the ferrous ones were not well resolvable at these *T*. Therefore, the parameters determined for them are less accurate. The results of all these calculations for which the *RA* of the S1 and S2 components are in good approximation the same and for which the Mössbauer parameters of all the subspectra show a consistent and physical acceptable dependence of temperature, are given in Table III. Figure 5 contains the experimental and calculated MS. It is clear that the area fractions of S1 and S2 decrease above 22 K.

4. Hyperfine field analysis

4.1 Temperature dependence of the hyperfine field

As is generally known, the *T*-dependence of the sublattice magnetisation (σ) in a classical magnetic structure can be described by a Brillouin curve within the molecular field theory of magnetism (Morrish 1965):

$$\sigma = B_{5/2}(\chi) = \frac{6}{5}\coth\left(\frac{6}{5}\chi\right) - \frac{1}{5}\coth\left(\frac{1}{5}\chi\right) \quad \text{with} \quad \chi = \frac{15}{7}\frac{T_N}{T}\sigma$$

Because the hyperfine field B_{hf} is in very good approximation proportional to the sublattice magnetization, here related to an iron site, the formula can also be applied to describe the *T*-dependence of B_{hf}:

$$\sigma = \frac{\mathrm{B_{hf}}(T)}{\mathrm{B_{hf}}(0K)} \quad \Leftrightarrow \quad \mathrm{B_{hf}}(T) = \mathrm{B_{hf}}(0K) \times B_{5/2}(\chi)$$

These $B_{\mathrm{hf}}(T)$ Brillouin curves are determined by the mean spin value of the probe-ions (2.5 for ferric ions), the saturation value of the magnetization at low temperatures (here: the hyperfine

field at lowest T) and the corresponding magnetic transition temperature (here: the T_N value as determined from thermoscanning). Figure 6 shows the experimental T-dependences of B_{hf} (most probable values) and the calculated Brillouin curves for the respective ferric sites and samples. It is clear that the molecular field model gives mostly only a raw description of the T-dependences of $B_{hf,S1}$ and $B_{hf,S2}$, and is totally deficient for $B_{hf,S3}(T)$. However for strunzite and ferrostrunzite a better description of $B_{hf,S1}$ and $B_{hf,S2}$ as function of T was obtained by a curve which takes into account the exchange magnetostriction associated with a non-second-order magnetic transition (Bean and Rodbell 1962). The argument of the Brillouin curve is than given by:

$$\chi = B_{5/2}^{-1}(\sigma) = [-2a - 4b\eta_{nso}\sigma^2]\frac{T_N}{T}\sigma$$
$$a = -\frac{15}{14} \qquad b = -\frac{2331}{9604}$$

Such a curve is calculated using an extra parameter, here noted by η_{nso} in order to distinguish it from the asymmetry parameter. η_{nso} is a measure for the departure from an ideal second-order magnetic transition and is determined by the fractional volume change at the transition, the compressibility, and the slope of the variation of the transition temperature with the lattice volume (Bean and Rodbell 1962). In the case of an ideal second-order magnetic transition η_{nso} = 0 and the curve is then the classical Brillouin curve; η_{nso} >1 corresponds to a first-order transition. η_{nso} can be determined by fitting this kind of curve to the experimental data using the same values for the other parameters as for the foregoing calculation of the corresponding classical Brillouin curve. Because the T-dependences of $B_{hf,S1}$ and $B_{hf,S2}$ are mutually very similar in strunzite, one finds η_{nso} = 0.43±0.01 for both S1 and S2 in the case of strunzite, and $\eta_{nso,S1}$ = 0.37±0.02 and $\eta_{nso,S2}$ = 0.34±0.02 in the case of ferrostrunzite, indicating that the magnetic transition at the corresponding T_N is not a pure second-order. For ferristrunzite the best agreement with the experimental data was obtained for η_{nso} = 0±0.02, yielding the

classical Brillouin curve. Because the fractional volume changes at the magnetic transition temperatures for strunzite and ferrostrunzite are not known, more quantitative data about compressibility and slope of the variation of the transition temperature with the lattice volume cannot be derived from the obtained values for η_{nso}. In ferrostrunzite (Figure 3) it can be seen that T_N(S1,S2) is different from T_N(S3,S6), demonstrating that different sublattices can have different magnetic transition temperatures.

4.2 Re-entrant spin glass behaviour

The $B_{hf,S3}$ T-dependence is remarkable. In strunzite (Figure 6) $B_{hf,S3}$ (most probable values) decreases strongly when T increases from 0 to about 20 K, after which $B_{hf,S3}$ decreases less quickly when T further increases up to T_N. This kind of T-dependence is typical for re-entrant spin glass behaviour (De Bakker et al. 1997). This phenomenon occurs in systems in which some spins, here the ferric ones at the Mn sites, are frustrated in the sense that they are liable to conflicting magnetic exchange interactions which never can be satisfied simultaneously for all interactions (Stein 1989). The kink in the curve determines the so-called spin glass freezing temperature (T_{sg}). In strunzite, T_{sg} is estimated at 21 ± 1 K. Above T_{sg}, the frustrated spins are in a local paramagnetic-like state, and $B_{hf,S3}(T)$ then reflects the normal course of the spontaneous magnetisation (of non-frustrated Fe^{3+} spins at the Mn site), which almost reaches its saturation value at T_{sg}. Below T_{sg}, the frustrated spins are frozen in and their contribution is superimposed on the mean spin value of the non-frustrated spins. Because the hyperfine field of the non-frustrated spins was approximately saturated at T_{sg}, $B_{hf,S3}(T)$ then mainly reflects the T-dependence of the frustrated spins (Huck and Hesse 1989). A less pronounced analogous tendency is determined for $B_{hf,S3}$ in ferristrunzite and ferrostrunzite.

More quantitative discussion about this phenomenon can only be done when more data concerning the T-dependence of the ferric hyperfine fields are determined and the magnetic

structure is better clarified. Complete strunzite-ferristrunzite and strunzite-ferrostrunzite solution series are interesting mineral series for further research on this subject.

5. Conclusion

Strunzite, ferristrunzite and ferrostrunzite exhibit Mössbauer spectra at temperatures below the magnetic ordering temperature that are rather complicated to analyze. The B_{hf} of the iron located at the Mn sites decreases more strongly with temperature than these of the Fe(1) and Fe(2) sites. When temperature increases sufficiently, the absorption lines of the dominant sextets become asymmetrical and broaden as a consequence of relaxation effects. In strunzite this becomes visible above 40 K, in ferristrunzite and ferrostrunzite already above about 17 K and 23 K respectively. The *T*-dependence of the hyperfine fields of the Fe^{3+}(1) and Fe^{3+}(2) sites in strunzite and ferrostrunzite is succesfully described by a model which takes exchange magnetostriction effects into account and shows that the magnetic transition is not of pure second order. However in ferristrunzite, a classical Brillouin dependence is more likely. The *T*-dependence of the hyperfine field of the Fe^{3+} at the Mn sites in strunzite is rather extraordinary and shows re-entrant spin glass behaviour.

Acknowledgements

The authors thank the Fund for Scientific Research – Flanders for the continuous financial support.

References

Bean, C.P. and Rodbell, D.S. (1962) Magnetic disorder as a first-order phase transformation. Physical Review, 126, 104-115.

Blume, M., Tjon, T.A. (1968) Mössbauer spectra in a fluctuating environment. Physical Review, 165, 446-461.

Chambaere, D. and De Grave, E. (1984) On the Néel temperature of β FeOOH : structural dependence and its applications. Journal of Magnetism and Magnetic Materials, 42, 263-268.

De Bakker, P.M.A., Vandenberghe, R.E., and De Grave, E. (1997) Magnetic phase diagram for the spinel ferrite series $MgFe_{2-x}Cr_xO_4$ and $Mg_{1-x}Zn_xFe_{1,5}Cr_{0,5}O_4$ as determined by Mössbauer Spectroscopy. Journal Physique IV 7 C1, 267.

Frondel, C. (1957) Strunzit, ein neues Eisen-Mangan-Phosphat. Neues Jahrbuch fur Mineralogie-Monatshefte, 222-226.

Fanfani, L., Tomassini, M., Zanazzi, P., and Zanzari, A.R. (1978) The crystal structure of strunzite, a contribution of the crystal chemistry of basic ferric manganous hydrated phosphates. Tschermaks Mineralogische und Petrographische Mitteilungen, 25, 77-87.

Hoy, G.R. and Chandra, S. (1967) Effective Field Parameters in Iron Mössbauer Spectroscopy. Journal of Chemical Physics, 47, 961-965.

Huck, B. and Hesse, J. (1989), Mössbauer effect spectroscopy on the re-entrant spin glass FeNiMn. Journal of Magnetism and Magnetic Materials, 78, 247-254.

Kündig, W. (1967) Evaluation of Mössbauer spectra for ^{57}Fe. Nuclear Instruments and Methods in Physics Research, 48, 219-228.

Morrish, A.H. (1965) The Physical Principles of Magnetism, 680 p. Wiley, New-York.

Peacor, D.R., Dunn, P.J., and Simmons, W.B. (1983) Ferrostrunzite, the ferrous analogue of strunzite from Mullica Hill, New Jersey. Neues Jahrbuch fur Mineralogie-Monatshefte, 524-528.

Stein, D.L. (1989) Spin glasses. Scientific American, 261 (July), 36-42.

Van Alboom, A. and De Grave, E. (2005) Mössbauer effect in natural strunzite, ferristrunzite and ferrostrunzite. Hyperfine Interactions 166, 679-685.

Vandenberghe, R.E., De Grave, E., and de Bakker, P.M.A. (1994) On the methodology of Mössbauer spectra. Hyperfine Interactions 83, 29-49.

Van Tassel, R. and De Grave, E. (1992) Ferrostrunzite from Arnsberg, Sauerland, Germany. Neues Jahrbuch fur Mineralogie-Monatshefte, 207-212.

Vochten, R. and De Grave, E. (1990) Mössbauer and infrared spectroscopic characterization of ferristrunzite from Blaton, Belgium. Neues Jahrbuch fur Mineralogie-Monatshefte, 176-190.

Vochten, R., De Grave, E., Van Springel, K., and Van Haverbeke, L. (1995) Mineralogical and Mössbauer spectroscopic study of some strunzite varieties of the Silbergrube, Waidhaus, Oberpfalz, Germany. Neues Jahrbuch fur Mineralogie-Monatshefte, 11-25.

Figure captions

Figure 1. Part of the crystallographic structure of strunzite viewed along the c axis (adapted from Fanfani 1978).

Figure 2. Mössbauer thermoscanning curves of the three strunzite varieties.

Figure 3a. Experimental and calculated MS for ferristrunzite at 4.2 K. S1: blue; S2: purple; S3: magenta; calculated MS: red. Parameters are in Table I.

Figure 3b. Experimental and calculated MS for ferristrunzite (left) and corresponding probability histograms for the hyperfine fields (right) at selected temperatures. S1: blue; S2: purple; S3: magenta; D1: orange; calculated MS: red. Parameters are in Table I.

Figure 4. Experimental and calculated MS for strunzite at selected temperatures. S1: blue; S2: purple; S3: magenta; D1: orange; D2: pink; calculated MS: red. Parameters are in Table II.

Figure 5a. Experimental and calculated MS for ferrostrunzite at 5 K and 10 K. S1: blue; S2: purple; S3: magenta; S4: orange; S5: green; calculated MS: red. Parameters are in Table III.

Figure 5b. Experimental and calculated MS for ferrostrunzite (left) and corresponding probability histograms for the hyperfine fields (right) at 22 K and at 28 K. S1: blue; S2: purple; S4: orange; S5: green; S6: pink; calculated MS: red. Values of the relevant Mössbauer parameters are listed in Table III.

Figure 6. *T*-dependence of the hyperfine fields (most probable values) in ferristrunzite, strunzite and ferrostrunzite. Dotted lines are calculated Brillouin curves. Full lines are calculated accounting for exchange magnetostriction (see text) (Bean and Rodbell 1962). S1: blue; S2: purple; S3: magenta; S6: pink.

TABLES

Table I. Mössbauer parameters for ferristrunzite below T_N at selected temperatures. See text for the meaning of the symbols. Except at T=4.2 K (errors in the last digit), estimated errors are: 0.5 K on T, 0.01 mm/s on δ, 0.05 mm/s on $2\varepsilon_Q$, 0.03 mm/s on ΔE_Q, 0.02 mm/s on Γ, 0.5 T on B_{max} (B_{hf} with maximum probability), 0.5% on RA. At 4.2 K the given widths refer to the outer lines of the sextets. SFP1 (single component fit program), DFP1 (distribution fit program) are both based on analytical expressions for the calculation of the absorption line positions. B_{hfmin}, B_{hfmax}, #div: underlimit, upperlimit and number of divisions of the distribution range of B_{hf} for use in DFP1.

T (K)	Progr	Comp	B_{hfmin} (T)	B_{hfmax} (T)	#div	B_{max} (T)	δ (mm/s)	$2\varepsilon_Q$ (mm/s)	ΔE_Q (mm/s)	Γ (mm/s)	RA (%)
4.2	SFP1	S1				48.4(1)	0.508(5)	-0.63(2)		0.48(1)	35
		S2				47.8(1)	0.508(5)	0.11(2)		0.42(1)	35
		S3				54.8(1)	0.498(5)	-0.22(2)		0.35(1)	30
17	DFP1	S1	35.0	45.5	23	41.7	0.51	-0.48		0.40	24
		S2	35.0	45.5	23	41.8	0.51	0.18		0.40	24
		S3	10.0	35.0	26	31.2	0.51	0.14		0.40	38
		D1					0.51		0.71	0.66	14
21	DFP1	S1	30.0	45.0	31	40.1	0.51	-0.46		0.37	22.5
		S2	30.0	45.0	31	40.4	0.51	0.16		0.37	22.5
		S3	10.0	35.0	26	24.4	0.51	0.18		0.37	37
		D1					0.51		0.74	0.58	18
29	DFP1	S1	20.0	40.0	21	33.8	0.51	-0.46		0.35	16
		S2	20.0	40.0	21	34.7	0.51	0.32		0.35	16
		S3	3.0	31.0	29	14.3	0.51	0.12		0.35	32
		D1					0.51		0.75	0.53	36
33	DFP1	S1	20.0	40.0	21	30.9	0.52	-0.42		0.31	14.5
		S2	20.0	40.0	21	31.6	0.52	0.32		0.31	14.5
		S3	3.0	31.0	29	12.3	0.52	0.17		0.31	29
		D1					0.52		0.76	0.39	42

Table II. Mössbauer parameters for strunzite below T_N. See text for the meaning of the symbols. Typical errors are: 0.5 K on T, 0.005 mm/s on δ, 0.005 mm/s on ΔE_Q and $2\varepsilon_Q$, 0.005 mm/s on Γ, 0.5 T on B_{max} (B_{hf} with maximum probability), 0.1 on x, 0.5% on RA. SFP1 (single component fit program), DFP1 (distribution fit program) are both based on analytical expressions for the calculation of the absorption line positions. B_{hfmin}, B_{hfmax}, #div: underlimit, upperlimit and number of divisions of the distribution range of B_{hf} for use in DFP1. For the discrete sextets, given line widths are for the outer lines. x is the line area ratio of the second (and fifth) line relative to the third (and fourth) line in a sextet. The line area ratio of the first (and sixth) line to the third (and the fourth) line of a sextet was always fixed at 3.

T (K)	Progr	Comp	B_{hfmin} (T)	B_{hfmax} (T)	#div	B_{max} (T)	δ (mm/s)	$2\varepsilon_Q$ (mm/s)	ΔE_Q (mm/s)	Γ (mm/s)	x	RA (%)
4.2	SFP1	S1				48.6	0.518	-0.425		0.436	2.2	43.3
		S2				48.3	0.518	0.078		0.436	2.2	43.3
		S3				54.2	0.501	0.177		0.490	2.2	10.8
		D2					0.316		0.330	0.802		2.6
10	SFP1	S1				47.2	0.519	-0.354		0.393	2.1	43.5
		S2				47.0	0.519	0.126		0.393	2.1	43.5
		S3				44.1	0.519	0.068		0.687	2.1	10.9
		D2					0.316		0.330	0.540		2.1
15	DFP1	S1				45.8	0.515	-0.240		0.381	2.0	42.8
		S2				45.8	0.515	0.185		0.381	2.0	42.8
		S3	30.0	45.0	31	37.5	0.515	0.413		0.236	2.0	12.0
		D2					0.316		0.330	0.510		2.4
20	DFP1	S1				44.6	0.507	-0.115		0.386	1.7	40.9
		S2				44.6	0.507	0.190		0.386	1.7	40.9
		S3	5.0	35.0	61	22.0	0.507	0.371		0.449	1.7	16.6
		D2					0.316		0.257	0.500		1.6
25	DFP1	S1				43.3	0.510	-0.112		0.384	1.7	41.2
		S2				43.1	0.510	0.197		0.384	1.7	41.2
		S3	0.0	25.0	51	16.7	0.510	0.449		0.250	1.7	17.6
30	DFP1	S1				41.6	0.510	-0.107		0.376	1.7	40.9
		S2				41.5	0.510	0.190		0.376	1.7	40.9
		S3	0.0	25.0	51	13.5	0.510	0.446		0.239	1.7	18.2
35	DFP1	S1				39.1	0.506	-0.100		0.381	1.7	40.0
		S2				38.9	0.506	0.206		0.381	1.7	40.0
		S3	0.0	25.0	51	11.4	0.506	0.376		0.256	1.7	20.0
40	DFP1	S1				35.3	0.508	-0.110		0.450	1.7	40.8
		S2				35.2	0.508	0.190		0.450	1.7	40.8
		S3	0.0	20.0	41	9.2	0.508	0.643		0.260	1.7	18.4
43	DFP1	S1	25.0	35.0	21	31.8	0.508	-0.117		0.231	1.8	39.8
		S2	25.0	35.0	21	31.5	0.508	0.223		0.231	1.8	39.8
		S3	0.0	12.0	25	6.9	0.508	0.550		0.231	1.8	20.4
47	DFP1	S1	15.0	28.0	14	24.5	0.518	-0.100		0.286	1.8	35.1
		S2	15.0	28.0	14	24.2	0.518	0.229		0.286	1.8	35.1
		S3	0.0	10.0	21	5.1	0.518	0.452		0.286	1.8	19.5
		D1					0.518		0.749	0.396		10.3

Table III. Mössbauer parameters for strunzite below T_N. See text for the meaning of the symbols. Typical errors are: 0.5 K on T, 0.01 mm/s on δ, 0.01 mm/s on ΔE_Q and $2\varepsilon_Q$, 0.10 on η , 0.01 mm/s on Γ, 5° on Ω, 0.5 T on B_{max} (B_{hf} with maximum probability), 0.5% on RA. SFP2 (single component fit program) and DFP2 (distribution fit program) are both based on the diagonalization of the full nuclear interaction hamiltonian. B_{hfmin}, B_{hfmax}, #div: underlimit, upperlimit and number of divisions of the distribution range of B_{hf} for use in DFP2.

T (K)	Progr	Comp	B_{hfmin} (T)	B_{hfmax} (T)	#div	B_{max} (T)	δ (mm/s)	$2\varepsilon_Q$ (mm/s)	ΔE_Q (mm/s)	η	Ω (°)	Γ (mm/s)	RA (%)
5	SFP2	S1				48.2	0.51	-0.30				0.54	35.8
		S2				47.9	0.51	0.10				0.54	35.8
		S3				55.3	0.51	0.16				0.30	2.7
		S4				21.8	1.37		3.04	0.30	80	1.02	10.9
		S5				28.6	1.37		2.52	0.30	80	1.02	14.8
10	SFP2	S1				47.4	0.51	-0.34				0.56	35.5
		S2				47.2	0.51	0.04				0.56	35.5
		S3				46.7	0.51	0.30				0.25	2.7
		S4				16.8	1.37		3.04	0.08	68	0.90	11.1
		S5				22.7	1.37		2.52	0.08	80	0.90	15.2
22	DFP2	S1	35.0	45.5	21	44.4	0.52	-0.17				0.39	33.3
		S2	35.0	45.5	21	44.0	0.52	0.06				0.39	33.3
		S4				8.7	1.37		3.04	0.09	76	0.59	12.1
		S5				9.0	1.37		2.52	0.09	85	0.59	14.2
		S6	0.0	10.0	20	7.1	0.52	0.76				0.39	7.1
28	DFP2	S1	30.0	43.0	26	41.4	0.51	-0.19				0.33	31.8
		S2	30.0	43.0	26	41.0	0.51	0.16				0.33	31.8
		S4				6.5	1.37		3.04	0.01	79	0.44	10.2
		S5				5.9	1.37		2.52	0.01	80	0.44	16.5
		S6	0.0	10.0	20	3.1	0.51	0.76				0.33	9.7

REVISION 1
FIGURES

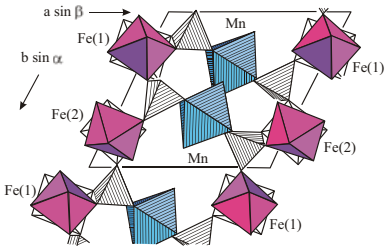

Figure 1.

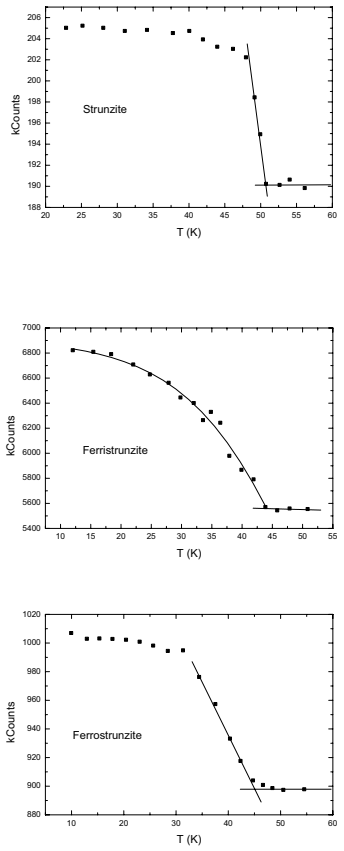
Strunzite
kCounts
T (K)
Ferristrunzite
kCounts
T (K)
Ferrostrunzite
kCounts
T (K)

Figure 2.

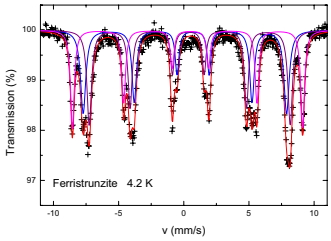

Figure 3a.

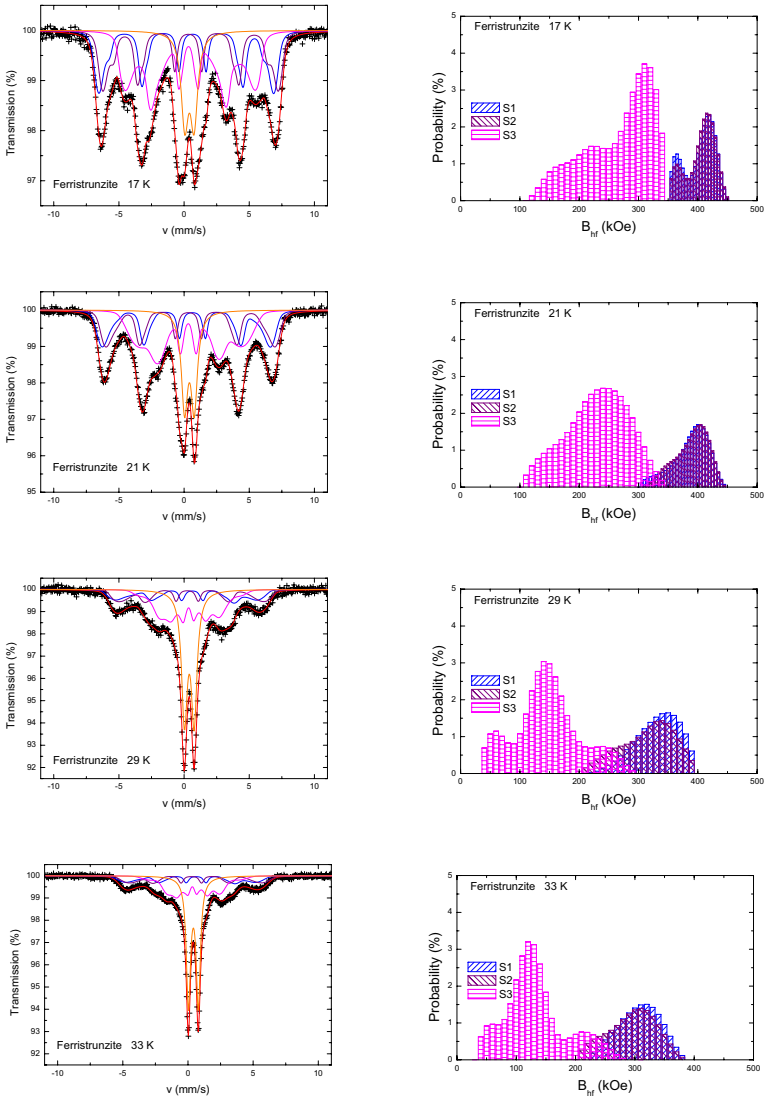

Figure 3b.

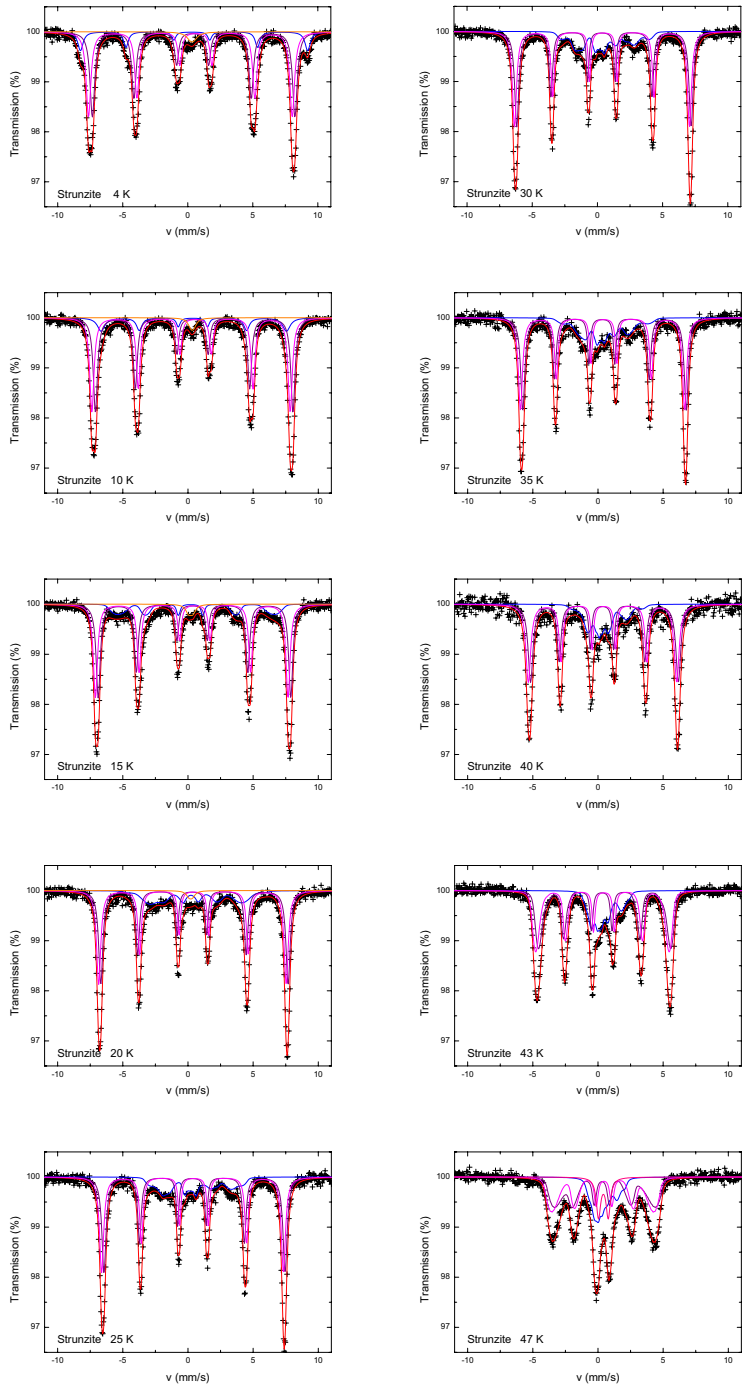
Strunzite 4 K
Strunzite 30 K
Strunzite 10 K
Strunzite 35 K
Strunzite 15 K
Strunzite 40 K
Strunzite 20 K
Strunzite 43 K
Strunzite 25 K
Strunzite 47 K
Transmission (%)
v (mm/s)

Figure 4.

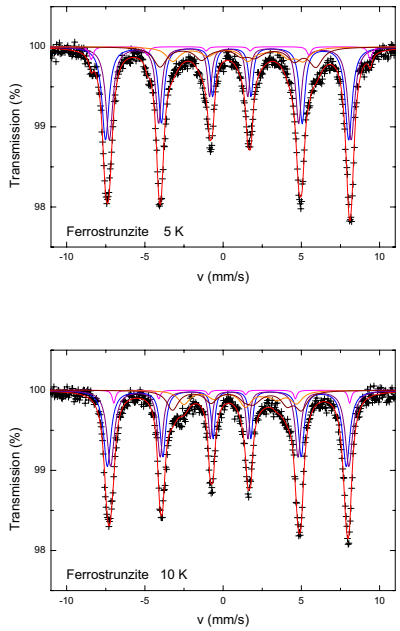

Figure 5a.

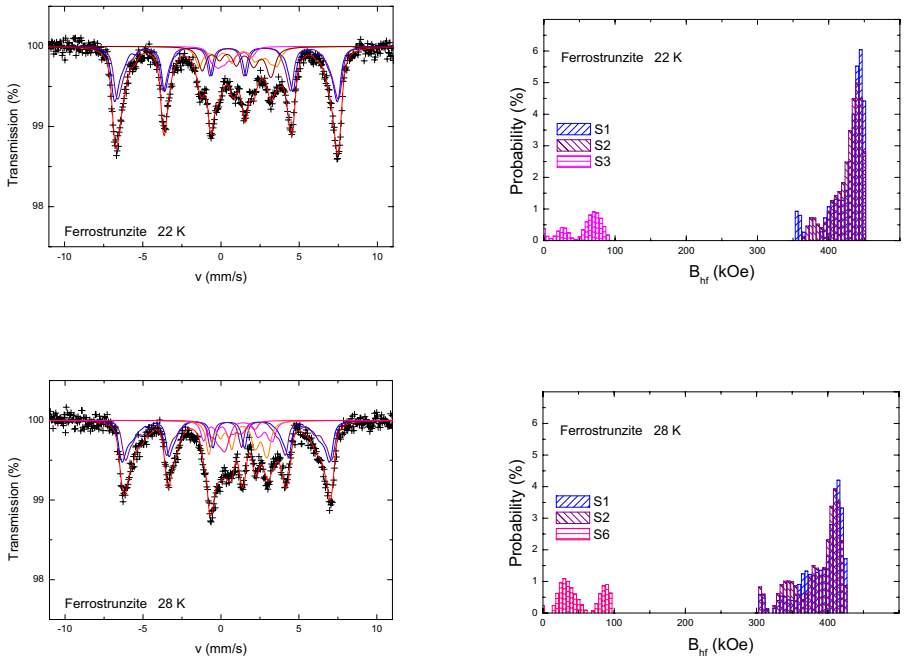

Figure 5b.

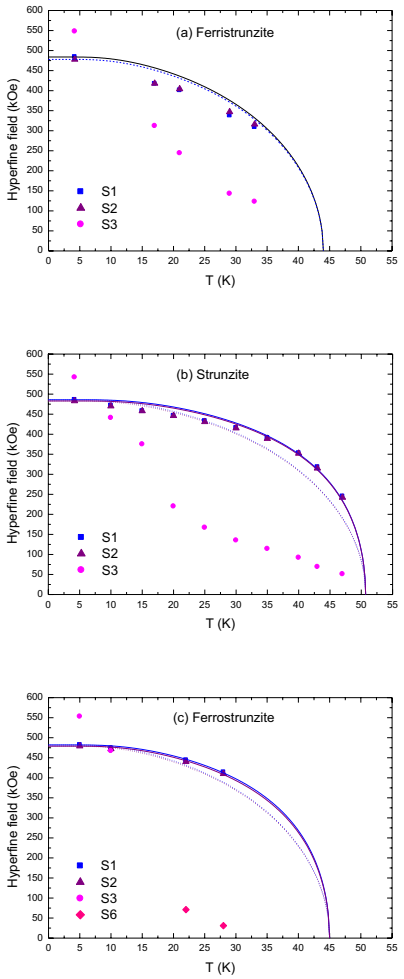
(a) Ferristrunzite
(b) Strunzite
(c) Ferrostrunzite
Hyperfine field (kOe)
T (K)
S1
S2
S3
S6

Figure 6.